The University of Reading
School of Mathematical and Physical Sciences

Solving Richards' equation using fixed and moving mesh schemes

by

Bruce Main

August 2011

This dissertation is a joint MSc in the Department of Mathematics and Statisitics & Department of Meteorology and is submitted in partial fulfilment of the requirements for the degree of Master of Science

Contents

Acknowledgements

After about 20 years this is my first time back into mathematics and its been very interesting and challenging! My classmates and various lecturers over the last two years have been very friendly and supportive so thanks go to them. Thanks goes to my workmates who have been most accommodating with time off work and working strange hours at times. Thanks also goes to the University of Reading for part-funding the masters. A special thanks to Louise for being very supportive of the two years while also having her own study to contend with. Most of all, thanks goes to my supervisor Mike Baines for all the positive meetings and help given. Many a time I have left his room with a considerably more positive frame of mind than when I entered, and plenty of notes.

Declaration

I confirm that this is my own work and the use of all materials from other sources have been properly and fully acknowledged.

Signed..... Date.....

1 Abstract

Richards' equation describing soil water flow is a highly nonlinear PDE and as such can only be solved numerically except for a small number of special conditions. Two schemes were considered here; the Crank Nicolson scheme with a nonlinear solver and a conservation-based moving mesh scheme. Four realistic scenarios were chosen to test the the schemes; i) a shallow moving water table, (ii) unsaturated infiltration on dry soil, (iii) ponded infiltration on dry soil, and (iv) infiltration into layered soil. The schemes were found to work well, with the ponded infiltration being the most challenging in terms of size of timestep required. Unstable flows were briefly considered where infiltrating water is held up momentarily. A mechanism for explaining this waiting time is described.

2 Introduction

The aim of this project was to implement a robust fixed mesh scheme and a conservative-based moving mesh (MM) scheme for solving Richards'equation (RE) for four realistic and challenging boundary conditions: (i) a shallow, moving water table, (ii) unsaturated infiltration, (iii) ponded infiltration, and (iv) infiltration into layered soil. Two soils were simulated which were chosen to be near the two ends of the textural spectrum; sandy and clayey soils. The fixed mesh scheme is the nonlinear Crank Nicolson (CNi) scheme which is a semi-implicit method requiring an iterative preocedure. Fixed mesh implicit schemes have been used extensively in the literature [4] for solving RE and more recently have incorporated time adaption schemes [5]. The performance of the CNi scheme and the requirement of adaptive timestepping is investigated here. The MM scheme investigated here is not a common form of the adaptive mesh schemes used for solving RE. Most adaptive mesh schemes are concerned with reducing truncation errors and increasing model effciency [6]. The advantage of the MM scheme is the inherent mass-conserving properties which is ideal for use in situations with moving boundaries such as moving water tables and infiltration.

In Chapter 2, the soil physics behind the RE is introduced and important variables such as soil water content (θ), soil water potential (ψ), and hydraulic conductivity (K) are defined and various relations involving these variables are described. The RE is derived and its various forms; ψ-based,

θ-based, and mixed, are given.

In Chapter 3, the schemes are described. The derivation of the CNi scheme starts with the explicit scheme and progresses to the linear Crank-Nicolson scheme (with K evaluated at the current time level) and finally on to the nonlinear Crank-Nicolson scheme (with K evaluated at the forward time level) with two methods of iteration described; Newton-Raphson and Picard. The explicit and linear Crank-Nicolson schemes are seen as natural building blocks for implementing the more complex nonlinear schemes. The discretisation at the boundaries for the four scenarios mentioned above is shown for the explicit method but related closely to that of the subsequent schemes. The MM scheme is derived along with the various boundary conditions mentioned above.

In Chapter 5 shows results of the simulations mainly in graphical form using the four scenarios above. The performance of the CNi scheme and the suitability of the MM scheme for solving RE is investigated. The size of the timestep used for the CNi scheme is analysed and comparisons between the two schemes shown. In Chapter 6, the concept of waiting times is investigated with reference to unstable flows. The MM scheme is used to numerically show the existence of a waiting time. Finally the project finishes with a Conclusions and Further Work chapter.

3 Background theory - soil physics

3.1 Soil Structure

Soil is a solid lattice made up of mineral and organic fractions. The mineral fraction generally makes up the majority by volume and consists of particles of diameters varying from clay ($> 2\ \mu m$) to coarse sand (up to 2 mm). The relative proportion of these particle sizes and organic matter (which acts as a glue to bond particles togther to form aggregates) largely determines the range of pore sizes present in the soil. It is this distribution of pore sizes that greatly influences water storage and movement.

Water can be present in soils in its three phases, but most often in the liquid and gaseous phases only. Water movement in soil is mainly due to vapour and liquid flows. Vapour flow dominates in dry conditions where soil pores are largely empty of liquid and vapour flows under gradients of water vapour and temperature. Under wet conditions liquid water in pores creates a pathway for flow between adjacent pores with flows driven by moisture gradients and gravity. Only liquid water flows are considered in this report.

3.2 Soil water - definitions

There are two main concepts related to describing the amount or state of water in soils; (i) volumetric water content, θ (m^3m^{-3}), and (ii) water potenial, ψ (Pa or m). The amount of water in soil is almost always presented on a volume basis as shown in the equation below:

$$\theta = \frac{\text{Volume of water}}{\text{total volume of soil}} \tag{3.1}$$

Water potential relates to the energy state of the water in the soil pores. A formal definition found in most soil physics text books for water potential is [12]: 'The work required to move water from a free state such as a lake into the soil at current moisture levels'. There are two main components of ψ; matric potential (ψ_m) and gravitational potential (ψ_g), where $\psi = \psi_m + \psi_g$. The ψ_m component dominates during unsaturated conditions and relates to the capilliary forces or attraction of water molecules to solid surfaces. It is often referred to as a 'suction' and has a negative value except if free water is present on the soil surface. The magnitude of ψ_m increases as the soil dries. The ψ_g component dominates under saturated conditions where θ is at or near maximum (water occupying all pore spaces). Here water moves down the soil profile under the force of gravity. The magnitude of ψ_g is relative to some reference point (usually the soil surface). For future reference, ψ will be used to refer to matric potential, since matric and gravitational potential are always treated separately.

3.3 Soil moisture characteristics

There is a continuum of soil types from heavy clay to very sandy soils and with every soil there is a unique relationship between ψ and θ. The figure below shows typical curves describing the $\psi(\theta)$ relationship or soil moisture

characteristics (SMC) spanning from sandy to clay soils. In figure (3.1),

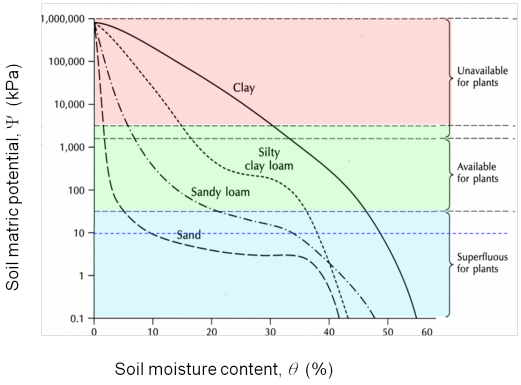

Figure 3.1: Typical SMCs for a range of soil types [1].

there are three shaded horizontal regions; (i)the blue region is the free-water zone where a portion of water drains from the soils under the force of gravity, (ii) the green region where water is now held in the soil against the force of gravity and some is available for plant uptake, and (iii) the red region which represents the residual water held very tightly in the pores. So for the two extreme soils, sand has most of its pore water loosely held and hence is drained away leaving $> 10\%$ left in the pores, and clay has about 50% still left in the red zone. The boundary between the blue and green regions is termed the 'field capacity', which represents the amount of water a soil can hold. The SMCs can be determined from in situ or laboratory measurements for each individual soil.

3.4 Empirical relations describing the SMC

The simplest empirical relation describing the SMCs in figure 3.1 above is the Brookes-Corey relation [2]:

$$\frac{\psi}{\psi_e} = \left(\frac{\theta}{\theta_s}\right) \tag{3.2}$$

where θ_s is the saturated value for θ (equivalent to the pore fraction in soil), ψ_e is termed the air-entry potential where $\theta = \theta_s$ for $\psi \geq \psi_e$, and b is the slope of equation 3.2 when log_e is applied to both sides. The parameter values for ψ_e and b are obtained either (i) from curve-fitting procedures if tabulated data for the SMC is available (most accurate), (ii) from other easily measured soil properties via various pedo-transfer functions, or (iii) from listed values in the literature for each soil type. The advantage of this relation is its simplicity and the easily understood correlations between b and ψ_e values with soil type. The main disadvantage is the poor way in which the SMCs are described near to saturation (see later in Figure 3.2). Another relation, devised by van Genuchten [3], improves the description of the SMC near to saturation as shown in Figure (3.2) and is given by:

$$S_e = \frac{\theta - \theta_r}{\theta_s - \theta_r} = \frac{1}{(1 + |\alpha\psi|^w)^f} \tag{3.3}$$

where S_e is the normalised water content, θ_r is the residual water content after air-drying, and α, w, and $f = 1 - 1/w$ are fitting parameters.

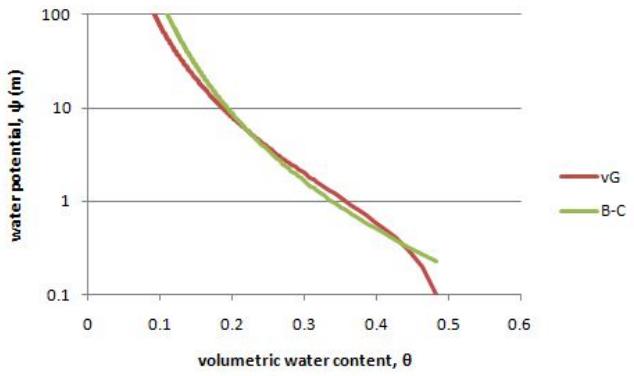

Figure 3.2: Comparison between van Genuchten (vG) and Brookes-Corey (B-C) formulations

3.5 Water flow in soils - Darcy's Law

The movement of water occurs in soil when gradients of ψ develop from inputs/removal of water from precipitation/evaporation at the soil surface or root uptake in the soil profile. Water flows from regions of high to low values of ψ and is described by Darcy's Law:

$$q = -K\left(\frac{\partial \psi}{\partial z} + 1\right) \tag{3.4}$$

where q is the flow rate (ms^{-1}), K is the hydraulic conductivity (ms^{-1}), and z is usually the depth below the soil surface (m). The hydraulic conductivity is a highly non-linear function of θ (or ψ) and is difficult to measure particularly at lower θ. However, K is found to be strongly connected to the SMC. Because of this, the expression for K is derived directly from expressions for the SMC, e.g. from equation (3.2):

$$K = K_s\left(\frac{\theta}{\theta_s}\right)^{n1} \qquad or \qquad K = K_s\left(\frac{\psi_e}{\psi}\right)^{n2} \tag{3.5}$$

where $n1 = 2b + 3$ and $n2 = 2 + 3/b$, and b is from equation (3.2).

3.6 Derivation of Richards' equation

The mass continuity equation

$$\frac{\partial q}{\partial z} = \frac{\partial \theta}{\partial t} \tag{3.6}$$

is combined with Darcy's Law (equation 3.4) to obtain Richards' equation (RE)

$$\frac{\partial \theta}{\partial t} = -\frac{\partial}{\partial z}\left[K\left(\frac{\partial \psi}{\partial z} - 1\right)\right]. \tag{3.7}$$

Root uptake is not considered here. Equation 3.7 is shown in 'mixed' form and is considered to be the natural form of RE where the quantity being

conserved is the physical quantity θ, the gradient being expressed in terms of ψ, and K is a function of θ. Other forms of RE are the θ-based and ψ-based versions shown below:

$$\begin{aligned} \frac{\partial \theta}{\partial t} &= -\frac{\partial}{\partial z}\left[K\left(D\frac{\partial \theta}{\partial z} - 1\right)\right] \\ C\frac{\partial \psi}{\partial t} &= -\frac{\partial}{\partial z}\left[K\left(\frac{\partial \psi}{\partial z} - 1\right)\right] \end{aligned} \tag{3.8}$$

where $D = \partial\psi/\partial\theta$ and $C = \partial\theta/\partial\psi$ from applying the product rule. The above forms of RE have been used extensively in the literature. The mixed and θ-based forms are best for conservation of mass, parrticularly when sharp moisture gradients are present, and the mixed and ψ-based forms are necessary for saturated conditions and layered soil [4]. During saturated conditions when water is ponding on the soil surface, the value of ψ at the surface equals the depth of free water on the surface. This positive potential cannot be portrayed using θ as the driving variable (equation 3.8a). For layered soil, ψ and not θ is the continuous variable down the soil profile.

3.7 Boundary conditions

For one dimensional vertical flow, only top and bottom boundary conditions exist as depicted in the schematic below (Figure 3.3). The top boundary or soil surface is exposed to the highly variable atmospheric conditions so can change rapidly. For the most part, the top boundary has a flux of water passing through it either downward from infiltration as liquid water or upward from evaporation in the vapour phase. If ponding does occur, when the precipitation rate is greater than the maximum infiltration rate (see later in next chapter), $\psi = h$ where h is the depth of water on the soil surface. When considering solving RE, the top boundary is predominantly

a Neumann or flux bounday condition, but for some soil types and environmental conditions, a Dirichlet boundary condition can occur. The bottom boundary is often deep enough such that the ψ gradient is considered to be zero, or for a shallow water table, the value of θ or ψ being equal to that at saturation.

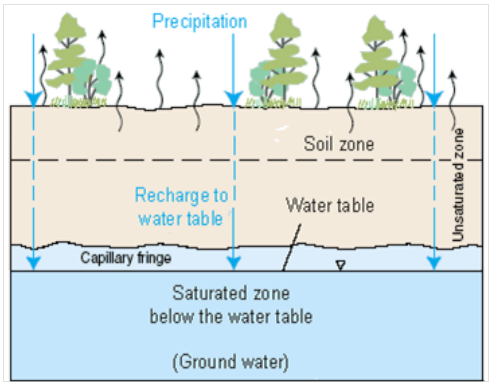

Figure 3.3: Schematic showing the vertical nature of water flows [1]

4 Numerical schemes for solving Richards' equation

Since the 1970's, inceasingly complex numerical schemes have been developed to solve RE. The highly non-linear nature of RE requires that numerical rather than exact solutions be sought. Due to the complex nature of real soils and environmental conditons, improvements to numerical schemes to increase the efficiency, stability and accuracy is ongoing. The schemes can be broadly grouped into schemes with fixed meshes (FM) and those with adaptive meshes (AM). The former are generally simpler to design and implement with the latter a relatively new concept. Only finite difference methods are investigated here since only one dimensional flows are considered. Techniques such as finite elements do not have appreciable advantages over finite differences in one dimension. This brief review on numerical schemes follows that of [5] who produced quite an extensive review on numerical solutions to RE. The fixed mesh methods used are a Crank-Nicolson linear scheme and a fully implicit nonlinear scheme using iterative methods such as Picard or Newton-Raphson [4]. These two methods are explored in more detail in the next section. A later improvement to these schemes was to add in an adaptive time-step procedure. Two main methods exist for varying the time step, h [6]; (i) empirical - based on the number of iterations per time step, and (ii) error-based where estimates of

the truncation error are obtained and the time step adjusted accordingly. In addition, the order of the time stepping scheme can be varied. The AM techniques can be grouped into three types; (i) moving mesh points, (ii) adding/subtracting mesh points, and (iii) increasing the order. Often a combination of the above techniques is used. As with the fixed mesh methods, adaptive time stepping can be included, producing some complex but robust schemes [5]. The main advantage of AM over FM schemes is the combination of increased accuracy and stability as well as efficiency. The FM schemes can be made more accurate by decreasing the distance between mesh points (Δz) and the time step, but this decreases the efficiency. With AM, h (and Δz) can be decreased only when required, which can be for relatively small periods of time. Larger h (and Δz) can be used for periods where little change is occuring to the soil water content (θ) or water potential (ψ). The disadvantage of most AM methods is their complexity so that they are harder than FM to implement. The added effort to develop such models may not be justified since the FM methods can suffice in many situations. The emphasis in this report is not to investigate the complex techniques developed but to implement a few of the popular FM schemes (see later in this chapter) and and analyse their performances under various situations (Results Chapter). For situations in soil where there is a moving shallow water table, as in river flood plains, or high rainfall areas where ponding causes a saturated zone to move downwards from the soil surface, a moving mesh technique can be used to track these moving boundaries. A velocity based moving mesh technique can be reasonably straightforward to implement and ideal for situations with moving boundaries [7]. Such a technique is investigated further in a later section.

4.1 Fixed mesh methods

Often at field-scale or larger, variation in the variables ψ and θ occurs mainly in the vertical dimension since horizontally the surface appears uniform. For larger scales, the region can be divided up into smaller areas of similar surface type, each with a one-dimensional flow scheme.

A mesh is first inserted on the vertical soil profile (z direction) usually with $z = 0$ at the soil surface (see figure 4.1 below). The spacings (Δz) often increase in the positive z direction with $\Delta z \approx 1$ cm at $z = 0$ and $\Delta z \approx 1$ m at the base of the profile. These spacings reflect the relative temporal and spatial variation of ψ and θ down the profile. The ψ-based RE (see previous chapter) is discretised in the following sections since it is used later in the Results chapter, but the analysis will be very similar for the other versions of RE. The rest of the chapter is devoted to the description of various simple numerical schemes for RE which can be represented here as $C\psi_t = (K(\psi_z - 1))_z$. The first and simplest is the explicit scheme where the first derivative in time (ψ_t) is approximated by the first order forward difference and the second order derivative in space approximated by a second order forward difference. The subsequent schemes investigated; various forms of the Crank-Nicolson scheme and fully implicit schemes, are based on this explicit discetisation.

Explicit scheme

The basic explicit discretisation of the ψ-based RE is

$$C\frac{\psi_i^{n+1} - \psi_i^n}{\Delta t} = \left[K^n_{i+\frac{1}{2}}\left(\frac{\psi^n_{i+1} - \psi^n_i}{\Delta z_i} - 1\right) - K^n_{i-\frac{1}{2}}\left(\frac{\psi^n_i - \psi^n_{i-1}}{\Delta z_i} - 1\right)\right]\frac{1}{\Delta \overline{z_i}} \tag{4.1}$$

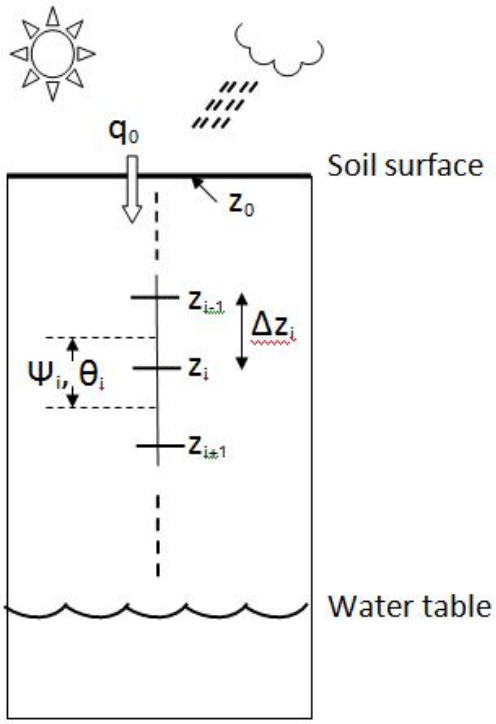

Figure 4.1: Soil profile divided into layers with ψ and θ centred on the mesh points.

where i and n are the space and time indices respectively, $\Delta z_i = z_i - z_{i-1}$, and $\Delta\overline{z_i} = 1/2(\Delta z_i + \Delta z_{i-1})$ (see Figure f41). This scheme is first order in time and second order in space and according to the stability criterion, the maximum timestep $\Delta t_{max} = 1/2\Delta z^2/K_{max}$. Equation (4.1) can be easily rearranged to have all the known terms (at nth timestep) on the RHS and ψ^{n+1} on the LHS. Values for ψ are obtained by advancing through time. Implementing this in code requires a space loop nested in a time loop.

The boundary conditions must be included. These are discussed below for the explicit method but equally apply to the subsequent schemes and can be readily implemented. Both the top and bottom boundaries for the

most part have Neumann conditions except for two special cases where; (i) at the top boundary, where ponding occurs at the soil surface, in which case $\psi_0 = h$, where h is the ponding depth, and (ii) where the bottom boundary coincides with a shallow water table, then $\psi_I = 0$. For the soil surface, the Neumann condition is:

$$C\frac{\psi_0^{n+1} - \psi_0^n}{\Delta t} = \left[K_{\frac{1}{2}}^n \left(\frac{\psi_1^n - \psi_0^n}{\Delta z_0} - 1\right) - q_0\right] \Delta\overline{z_0} \tag{4.2}$$

where q_0 is equal to the evaporation (e) or precipitation (p) rate (provided that $p < In_{max}$, where In_{max} is the maximum infiltration rate). Where $p > In_{max}$, ponding occurs and a Dirichlet boundary condition is implemented:

$$C_1\frac{\psi_1^{n+1} - \psi_1^n}{\Delta t} = \left[K_{\frac{3}{2}}^n \left(\frac{\psi_2^n - \psi_1^n}{\Delta z_0} - 1\right) - K_{\frac{1}{2}}^n \left(\frac{\psi_1^n - h}{L} - 1\right)\right] \Delta\overline{z_0} \tag{4.3}$$

where h is substituted in for ψ_0, L is the depth to the wetting front (see figure 4.2) and $L = \Delta z_0$ initially. As the ponding condition continues, L increases as subsequent θ_i values become equal to the saturated value. At the bottom boundary, the Neumann condition is:

$$C_I\frac{\psi_I^{n+1} - \psi_I^n}{\Delta t} = \left[K_I^n - K_{I-\frac{1}{2}}^n \left(\frac{\psi_I^n - \psi_{I-1}^n}{\Delta z_I} - 1\right)\right] \frac{1}{\Delta\overline{z_I}} \tag{4.4}$$

where I is the number of mesh points. When both boundary conditions are Neumann, there are $I+1$ equations and $I+1$ unknowns, whereas a Dirichlet boundary condition reduces the number of equations and unknowns by one.

Crank-Nicolson - linear scheme

The Crank-Nicolson discretisation of equation (4.5) is

$$C_i^n\frac{\psi_i^{n+1} - \psi_i^n}{\Delta t} = \frac{\Theta}{\Delta\overline{z_i}}\left[K_{i+\frac{1}{2}}^n \left(\frac{\psi_{i+1}^n - \psi_i^n}{\Delta z_i} - 1\right) - K_{i-\frac{1}{2}}^n \left(\frac{\psi_i^n - \psi_{i-1}^n}{\Delta z_i} - 1\right)\right]$$

$$+ \frac{1-\Theta}{\Delta\overline{z_i}}\left[K_{i+\frac{1}{2}}^n \left(\frac{\psi_{i+1}^{n+1} - \psi_i^{n+1}}{\Delta z_i} - 1\right) - K_{i-\frac{1}{2}}^n \left(\frac{\psi_i^{n+1} - \psi_{i-1}^{n+1}}{\Delta z_i} - 1\right)\right] \tag{4.5}$$

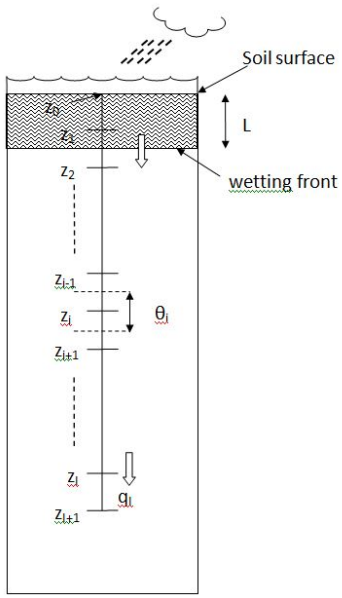

Figure 4.2: Schematic showing ponded infiltration into soil.

where $\Theta = 1/2$. This scheme is 2nd order in time and space. Note that for $\Theta = 0$, equation (4.5) reverts back to the explicit scheme of equation (4.1). The K terms are evaluated at timestep n so equation (4.5) is still a set of linear algebraic equations as with the explicit scheme above. However, the RHS contains $n+1$ terms so some rearranging of equation (4.5) is required to separate the n (on RHS) and the $n+1$ (on LHS) terms:

$$a_i^n \psi_{i-1}^{n+1} + b_i^n \psi_i^{n+1} + c_i^n \psi_{i+1}^{n+1} = r_i^n \tag{4.6}$$

where

$$a_i^n = -\frac{\Delta t K^n_{i-\frac{1}{2}}}{C_i^n \Delta z_{i-1} \Delta \overline{z_i}}(1-\Theta)$$

$$b_i^n = 1 + (1-\Theta)\frac{\Delta t K^n_{i-\frac{1}{2}}}{C_i^n \Delta z_{i-1} \Delta \overline{z_i}} - (1-\Theta)\frac{\Delta t K^n_{i+\frac{1}{2}}}{C_i^n \Delta z_i \Delta \overline{z_i}}$$

$$c_i^n = -\frac{\Delta t K^n_{i+\frac{1}{2}}}{C_i^n \Delta z_i \Delta \overline{z_i}}(1-\Theta)$$

$$r_i^n = \psi_i^n \frac{\Theta}{C_i^n \Delta \overline{z_i}} \left[K^n_{i+\frac{1}{2}} \left(\frac{\psi^n_{i+1} - \psi^n_i}{\Delta z_i} - 1 \right) - K^n_{i-\frac{1}{2}} \left(\frac{\psi^n_i - \psi^n_{i-1}}{\Delta z_i} - 1 \right) \right]$$
$$- \frac{\Delta t K^n_{i+\frac{1}{2}}}{C_i^n \Delta \overline{z_i}} + \frac{\Delta t K^n_{i-\frac{1}{2}}}{C_i^n \Delta \overline{z_i}}$$

This can all be written in matrix form:

$$\mathbf{A}\underline{\psi} = \underline{\mathrm{r}}$$

where

$$\mathbf{A} = \begin{pmatrix} b_0 & c_0 & 0 & \dots & & 0 \\ a_1 & b_1 & c_1 & & & \vdots \\ 0 & \ddots & \ddots & \ddots & & 0 \\ \vdots & & & a_{I-1} & b_{I-1} & c_{I-1} \\ 0 & \dots & & 0 & a_I & b_I \end{pmatrix}$$

In (A) above, a_i,b_i, and c_i terms make up the lower, middle and upper diagonals of $\mathbf{A}$ respectively. The vector $\underline{\psi}$ holds the ψ_i^{n+1} variables and $\underline{r}$ holds the known variables (at time level n) plus boundary conditions. Since $\mathbf{A}$ is tridiagonal (see above) and $|b_i| > |a_i| + |c_i|$, $\mathbf{A}$ is diagonally dominant and hence it is non-singular, and efficient algorithms such as the Thomas Algorithm can be used to solve for $\underline{\psi}$. As with the explicit scheme, the boundary conditions (along with the number of mesh points, I) determine the rank of $\mathbf{A}$, or the number of equations and unknowns. With both the

top and bottom boundary Neumann conditions, the rank of $\mathbf{A}$ is $I+1$ as shown. Implementation involves constructing $\mathbf{A}$ and $\underline{r}$ and solving for $\underline{\psi}$ at each timestep.

Crank-Nicholson - nonlinear scheme

A more implicit Crank-Nicolson scheme calculates the K and C terms in equation (4.5) at the $n+1/2$ time level:

$$K_{i+\frac{1}{2}}^{n+\frac{1}{2}} = \Theta K_{i+\frac{1}{2}}^{n} + (1-\Theta)K_{i+\frac{1}{2}}^{n+1} \quad \text{and} \quad C_{i}^{n+\frac{1}{2}} = \Theta C_{i}^{n} + (1-\Theta)C_{i}^{n+1} \tag{4.7}$$

The full discretisation is otherwise the same as equation (4.5). Two of the more popular iterative procedures for solving the resulting set of nonlinear equations are Picard and Newton-Raphson methods. With the iteration index as p, the Picard method has the ψ terms at the $p+1$ level and K and C at level p as shown below in equation (4.8):

$$C_{i}^{n+\frac{1}{2},p}\frac{\psi_{i}^{n+1,p+1}-\psi_{i}^{n}}{\Delta t} = \frac{\Theta}{\Delta\overline{z_i}}\left[K_{i+\frac{1}{2}}^{n+\frac{1}{2},p}\left(\frac{\psi_{i+1}^{n}-\psi_{i}^{n}}{\Delta z_i}-1\right) - K_{i-\frac{1}{2}}^{n+\frac{1}{2},p}\left(\frac{\psi_{i}^{n}-\psi_{i-1}^{n}}{\Delta z_i}-1\right)\right]$$

$$+\frac{1-\Theta}{\Delta\overline{z_i}}\left[K_{i+\frac{1}{2}}^{n+\frac{1}{2},p}\left(\frac{\psi_{i+1}^{n+1,p+1}-\psi_{i}^{n+1,p+1}}{\Delta z_i}-1\right) - K_{i-\frac{1}{2}}^{n+\frac{1}{2},p}\left(\frac{\psi_{i}^{n+1,p+1}-\psi_{i-1}^{n+1,p+1}}{\Delta z_i}-1\right)\right] \tag{4.8}$$

This essentially linearises the scheme so that the procedure shown in the previous section for the non-iterative Crank-Nicolson method can be used here except $\mathbf{A}$ and $\underline{r}$ are updated at each iteration level. Note that for $\Theta = 0$, this gives the fully implicit scheme, and $\Theta = 1$ gives the explicit scheme. The Newton method is based on the following algorithm:

$$\mathbf{J}\left[\underline{\psi}^{n+1,p+1} - \underline{\psi}^{n+1,p}\right] = -\underline{F} \tag{4.9}$$

where $\mathbf{J}$ is the Jacobian matrix which is shown below with Neumann boundary conditions (rank $= I+1$) and $\underline{F}$ is a vector with all the terms calcu-

lated at the previous iteration step. As the iteration proceeds, $\underline{F} \to 0$ as $\underline{\psi}^{n+1,p+1} \to \underline{\psi}^{n+1,p}$. The elements of $\mathbf{J}$ are calculated at the p iteration level.

$$\mathbf{J} = \begin{pmatrix} \frac{\partial F_0}{\partial \psi_0} & \frac{\partial F_0}{\partial \psi_1} & 0 & \dots & & 0 \\ \frac{\partial F_1}{\partial \psi_0} & \frac{\partial F_1}{\partial \psi_1} & \frac{\partial F_1}{\partial \psi_2} & & & \vdots \\ 0 & \ddots & \ddots & \ddots & & 0 \\ \vdots & & & \frac{\partial F_{I-1}}{\partial \psi_{I-2}} & \frac{\partial F_{I-1}}{\partial \psi_{I-1}} & \frac{\partial F_{I-1}}{\partial \psi_I} \\ 0 & \dots & & 0 & \frac{\partial F_I}{\partial \psi_{I-1}} & \frac{\partial F_I}{\partial \psi_I} \end{pmatrix}$$

The elements of $\underline{F}$ are calculated at the n and $n + 1/2, p$ levels.

$$F_i = \psi_i^{n+1,p} - \psi_i^n + \frac{\Delta t \Theta}{C_i^{n+\frac{1}{2},p} \Delta \overline{z_i}} \left[K_{i+\frac{1}{2}}^{n+\frac{1}{2},p} \left(\frac{\psi_{i+1}^n - \psi_i^n}{\Delta z_i} - 1 \right) - K_{i-\frac{1}{2}}^{n+\frac{1}{2},p} \left(\frac{\psi_i^n - \psi_{i-1}^n}{\Delta z_i} - 1 \right) \right]$$

$$+ \frac{(1-\Theta)\Delta t}{C_i^{n+\frac{1}{2},p} \Delta \overline{z_i}} \left[K_{i+\frac{1}{2}}^{n+\frac{1}{2},p} \left(\frac{\psi_{i+1}^{n+1,p} - \psi_i^{n+1,p}}{\Delta z_i} - 1 \right) - K_{i-\frac{1}{2}}^{n+\frac{1}{2},p} \left(\frac{\psi_i^{n+1,p} - \psi_{i-1}^{n+1,p}}{\Delta z_i} - 1 \right) \right] \tag{4.10}$$

The matrix $\mathbf{J}$ is diagonally dominant and hence non-singular, so can be inverted to solve equation 4.9.

4.2 Moving mesh - velocity based

A moving mesh scheme using a velocity-based approach is also applied to the vertical soil profile. This type of scheme is particularly useful where there are moving boundaries in the physical system. For the soil environment, two such cases exist: (i) a moving water table at the bottom boundary, and (ii) ponded infiltration at the top boundary. The former can occur in areas such as flood plains or water meadows where the water table (depth below soil surface) is largely driven by the river levels nearby. The water table can therefore fluctuate relatively quickly. Ponded infiltration occurs when the rate of rainfall is greater than the maximum rate of infiltration for the

soil considered. Water ponds on the soil surface while below the surface the water infiltrates with a sharp wetting front. This wetting front moves down the soil profile all the while that ponding exists at the surface. It must be noted here that this moving mesh method would not be viable for a layered soil where there would be stationary boundaries in the soil profile. Therefore the analysis is restricted to a homogenous soil.

Consider a uniform soil profile (see Figure 4.3) with a uniform mesh inserted between the soil surface (top boundary, a) and the top of the water table (bottom boundary, b). Neumann conditions exist at both boundaries where evaporation and infiltration occurs at the top, while drainage or influx from water table occurs at the bottom. A conservation-based moving mesh scheme is derived below following [7] and [8]. The main strategy behind the moving mesh concept is to keep the fractional amount of water between adjacent mesh points constant, i.e., $(z_i - z_{i-1})\theta_i$ is constant. This is the same as writing:

$$\frac{\int_a^{z_i(t)} \theta dz}{\int_a^b \theta dz} = \gamma_i \tag{4.11}$$

where α_i is constant in time. Differentiating equation (4.11) and substituting in γ_i:

$$\begin{aligned} 0 &= \frac{-\frac{\partial}{\partial z}\int_a^b \theta dz}{\left[\int_a^b \theta dz\right]^2} \int_a^{z_i(t)} \theta dz + \frac{\partial}{\partial z \int_a^{z_i(t)} \theta dz} \int_a^b \theta dz \qquad (4.12) \\ &= \frac{-\partial}{\partial z} \int_a^{z_i(t)} \theta dz \gamma_i + \int_a^{z_i(t)} \theta dz. \qquad (4.13) \end{aligned}$$

Using Leibniz rule:

$$\frac{d}{dt}\int_a^{z_i(t)} \theta dz = \int \left[\frac{\partial \theta}{\partial t} + \frac{\partial}{\partial z}\left(\theta \frac{dz}{dt}\right)\right] dz$$

and substituting into equation (4.13) the following is obtained:

$$\gamma_i \int_a^b \left[\frac{\partial \theta}{\partial t} + \frac{\partial}{\partial z}\left(\theta \frac{dz_i}{dt}\right)\right] dz = \int_a^{z_i(t)} \left[\frac{\partial \theta}{\partial t} + \frac{\partial}{\partial z}\left(\theta \frac{dz_i}{dt}\right)\right] dz. \tag{4.14}$$

RE, e.g., the mixed version [9], can now be substituted into equation (4.14) to get:

$$\gamma_i \int_a^b \left\{ \frac{\partial}{\partial z}\left[K\frac{\partial \psi}{\partial z} - 1\right] + \frac{\partial}{\partial z}\left(\theta \frac{dz_i}{dt}\right)\right\} dz$$

$$= \int_a^{z_i(t)} \left\{ \frac{\partial}{\partial z}\left[K\frac{\partial \psi}{\partial z} - 1\right] + \frac{\partial}{\partial z}\left(\theta \frac{dz_i}{dt}\right)\right\} dz. \quad (4.15)$$

Expanding the integrals in equation (4.15)

$$\left[K\frac{\partial \psi}{\partial z} - 1\right]_a^b \gamma_i + \left[\theta \frac{dz_i}{dt}\right]_a^b \gamma_i = \left[K\frac{\partial \psi}{\partial z} - 1\right]_a^{z_i(t)} + \left[\theta \frac{dz_i}{dt}\right]_a^{z_i(t)} \quad (4.16)$$

and rearranging equation (4.16), an expression for dz/dt is found:

$$\frac{dz}{dt} = \frac{1}{\theta}\left\{\gamma_i \left(\left[K\frac{\partial \psi}{\partial z} - 1\right]_a^b + \left[\theta \frac{dz_i}{dt}\right]_a^b\right) - \left[K\frac{\partial \psi}{\partial z} - 1\right]_a^{z_i(t)} + \left[\theta \frac{dz_i}{dt}\right]_a\right\} \quad (4.17)$$

Boundary conditions need to be applied to equation (4.17). Three possible scenarios are considered here which apply to the moving mesh method:

(i) fixed Neumann boundary condition at a, and a free Neumann boundary at b

(ii) fixed Neumann boundary condition at a, and a Neumann boundary at b which coincides with the top of the water table

(iii) Neumann boundary condition at a coinciding with the base of the wetting front from surface ponding, and a free Neuamnn boundary at b

Figure 4.3 below shows a mesh inserted on the soil profile and the scenarios illustrated. Inserting the boundary conditions for scenario (i), equation

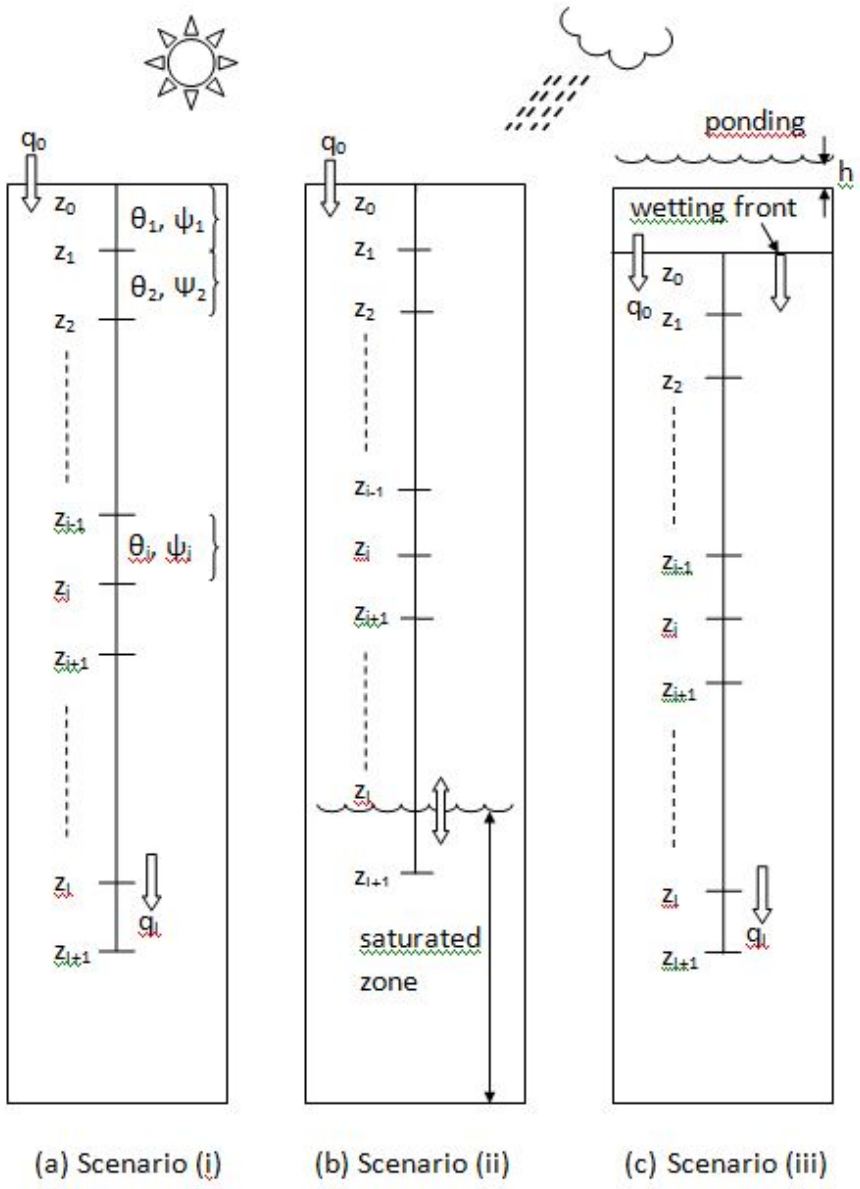

Figure 4.3: Moving mesh scheme illustrated for the three scenarios described in the text.

(4.17) becomes:

$$\frac{dz_i}{dt} = \frac{1}{\theta}\left\{\gamma\left(\left[K\frac{\partial\psi}{\partial z} - 1\right]^b - e\right) - \left[K\frac{\partial\psi}{\partial z} - 1\right]^{z_i} + e\right\} \tag{4.18}$$

where $da/dt = 0$ and $db/dt = 0$ since there is no imposed boundary velocities and e is the prescribed boundary condition at a which is set by the external atmospheric conditions. For scenario (ii), equation (4.17) becomes:

$$\frac{dz_i}{dt} = \frac{1}{\theta}\left\{\gamma_i\left(\left[K\frac{\partial\psi}{\partial z} - 1\right]^b - e + \theta_b\frac{\partial b}{\partial t}\right) - \left[K\frac{\partial\psi}{\partial z} - 1\right]^{z_i(t)} + e\right\} \tag{4.19}$$

where $\partial b/\partial t$ is the velocity of the top of the moving water table and θ_b is the value of θ at b. Finally for scenario (iii),

$$\frac{dz_i}{dt} = \frac{1}{\theta}\left\{\gamma_i\left(\left[K\frac{\partial\psi}{\partial z} - 1\right]^b - e - \theta_a\frac{\partial a}{\partial t}\right) - \left[K\frac{\partial\psi}{\partial z} - 1\right]^{z_i(t)} + e + \theta_a\frac{\partial a}{\partial t}\right\} \tag{4.20}$$

The equations (4.18)-(4.20) show how the mesh points move under the scenarios (i)-(iii). Discretisation of equation (4.18) (equations (4.19) and (4.20) are similarly discretised but not shown here) is given by:

$$\frac{z_i^{n+1} - z_i^n}{\Delta z_i^n} = \frac{1}{\theta_i}\left\{\gamma_i\left(K^n_{I+\frac{1}{2}}\left[\frac{\psi^n_{I+1} - \psi^n_I}{\Delta\overline{z^n_I}} - 1\right] - e^n\right) - K^n_{i+\frac{1}{2}}\left[\frac{\psi^n_{i+1} - \psi^n_i}{\Delta\overline{z^n_i}} - 1\right]\right\} \tag{4.21}$$

where $\Delta z_i = z_{i-1} - z_i$ and $\Delta\overline{z_i} = 1/2(\Delta z_i + \Delta z_{i+1})$. The $K^n_{i+\frac{1}{2}}$ is given by:

$$K^n_{i+\frac{1}{2}} = \frac{\alpha K^n_i + \beta K^n_{i+1}}{\alpha + \beta} \tag{4.22}$$

where $\alpha = 1/2\Delta z^n_i$ and $\beta = 1/2\Delta z^n_{i+1}$. The change in the amount of water in the soil profile (dW/dt) after each timestep is given by

$$\frac{dW}{dt} = K^n_{I+\frac{1}{2}}\left[\frac{\psi^n_{I+1} - \psi^n_I}{\delta\overline{z^n_I}} - 1\right] - e^n. \tag{4.23}$$

To implement this scheme, an initial profile of θ_i is given. In a time loop, the values ψ^n_i and $\overline{K}^n_i$ are calculated followed by $\partial z^n_i/\partial t$ for the current

timestep. New values for z_i and W at the next timestep are found by the fourth order Runga-Kutta time stepping scheme to improve the accuracy (and stability to a small degree) from Euler's first order explicit method. Values for θ_i^{n+1} are calculated using equation (4.11) in the discretised form

$$\theta_i^{n+1} = (\gamma_i - \gamma_{i-1}) \frac{W}{\Delta z_i}.$$

5 Solutions to Richards' equation

This chapter mainly focusses on the performances of the nonlinear iterative Crank Nicolson (CNi) and moving mesh (MM) schemes under various realistic situations:

(i) moving water table near the soil surface

(ii) infiltration into dry soil; unsaturated and ponded infiltration

(iii) infiltration into layered soil

The above cases represent some of the more challenging areas in soil water flow with respect to model stability and accuracy. The output from the other schemes described in the previous chapter give similar results to the CNi scheme provided suitable timesteps are applied. The Newton Raphson iteration method is mainly considered here with the Picard method giving virtually identical results but with more iterations required [10]. The sizes of timestep chosen here is a compromise between accurate solutions and efficient use of computer resource. An hourly timestep is chosen whenever possible as this gives good diurnal resolution and will generally give good results in most situations [11]. The size of the timestep used in the following analysis depends on the level of accuracy calculated.

5.1 Moving water table

Situations occur such as on a floodplain when there exists a shallow water table which varies according to the height and flow of the nearby river. Here the depth of the water table is modelled by a sinusoidal function imitating increasing and retreating river levels as a result of a large rainfall event inside the catchment. Figures 5.1 and 5.2 below illustrate the movement of the water table with time in relation to the soil profile. Here at the

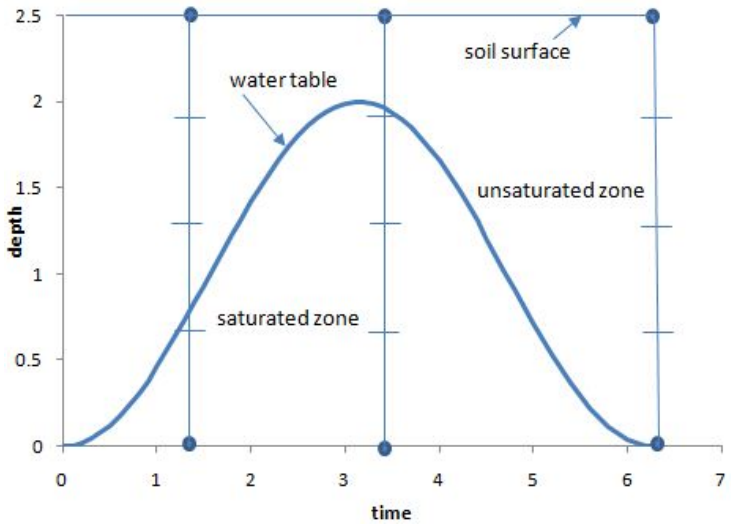

Figure 5.1: Sinusoidally varying water table with the fixed mesh scheme.

stationary top boundary, evaporation is allowed to occur at a rate given by:

$$e = \frac{-4}{8.64 \times 10^7} \frac{\theta_0}{\theta_s} \tag{5.1}$$

where the maximum rate is set at 4 $mm\ day^{-1}$ and regulated by the amount of water in the top layer. For the fixed mesh schemes, the location of the water table is achieved using interpolation. The moving mesh scheme has a mesh point located on the water table and this tracks its movement. Figures 5.3 and 5.4 shows results from the CNi scheme for two contrasting

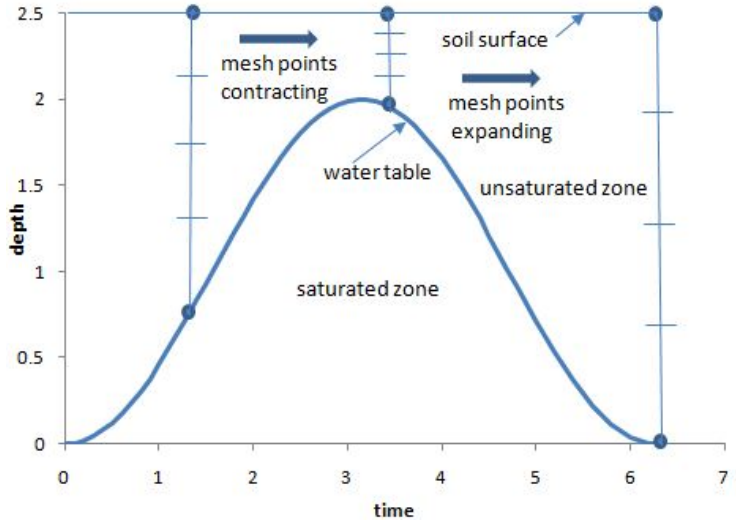

Figure 5.2: Sinusoidally varying water table with the moving mesh scheme.

soil types; a sandy and clayey soil. Table 5.1 below shows values for typical soil hydraulic parameters. The timesteps chosen were $600s$ for the sandy

Table 5.1: Parameter values.

	Sandy soil	Clayey soil	units
K_s	50	2	$mmhr^{-1}$
θ_s	0.43	0.5	m^3m^{-3}
b	3.0	8.0	$-$
ψ_e	-0.1	-0.5	m

soil and $3600s$ for the clayey soil simulations. A measure of the accuracy of the simulations are shown in Table 5.2 which were calculated by comparing to a simulation with small Δt and Δz values. Figures 5.5 and 5.6 show the results from the MM scheme with the bottom mesh point coinciding with the water table. The moving mesh tracks the varying water table as shown in figure 5.7 but the results differ slightly from the fixed mesh scheme near the top boundary. The reason for this is uncertain, however a water balance

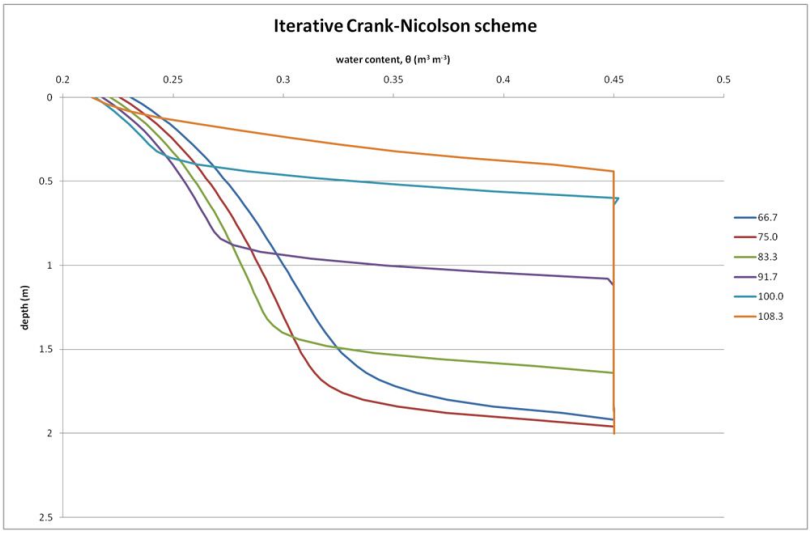

Figure 5.3: Results from fixed mesh schemes with varying water table for sandy soils.

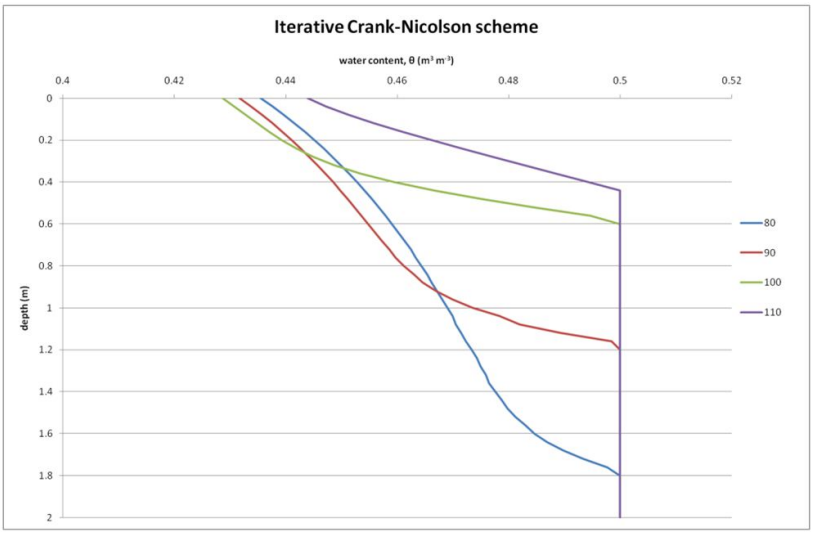

Figure 5.4: Results from fixed mesh schemes with varying water table for clayey soils.

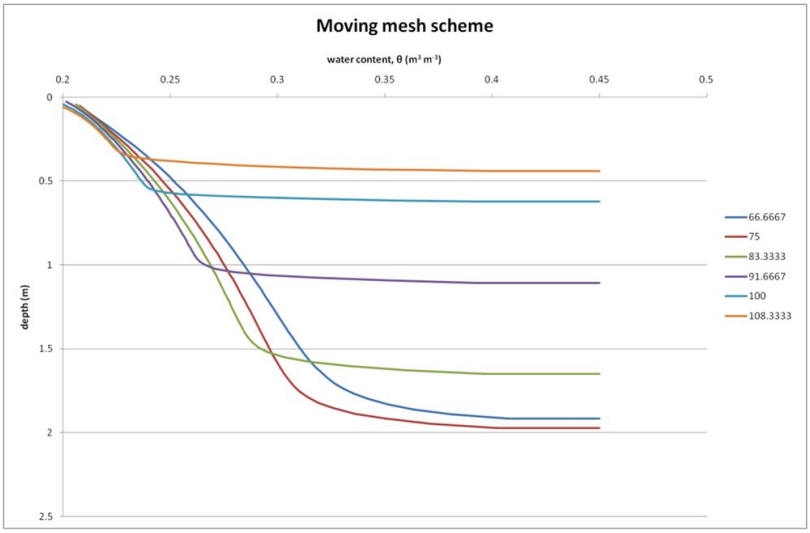

Figure 5.5: Results from moving mesh scheme with varying water table for sandy soil.

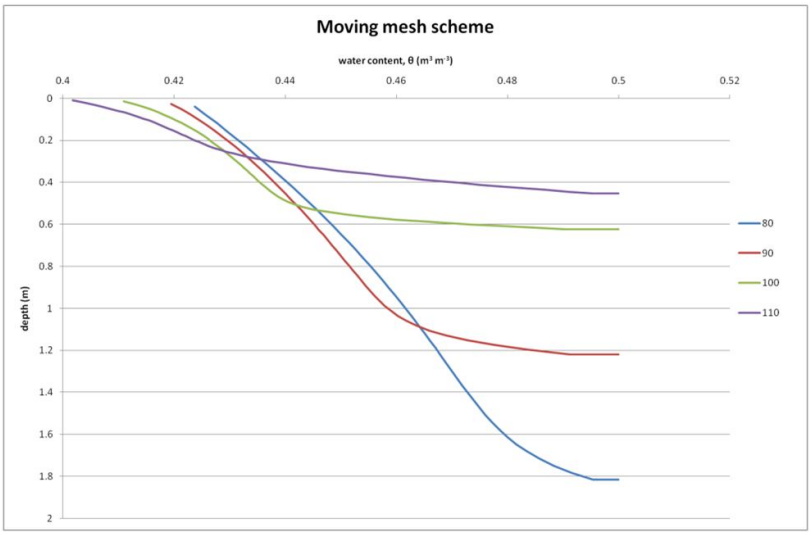

Figure 5.6: Results from moving mesh scheme with varying water table for clayey soil.

Table 5.2: % error values in profile water between the schemes.

time(hr)	z_w (m)	% error sand	% error clay
10	1.71	1.70	1.50
20	1.07	1.60	1.57
30	0.53	1.40	1.60
40	0.47	1.22	1.49
50	0.94	1.18	1.40
100	0.61	1.50	1.74

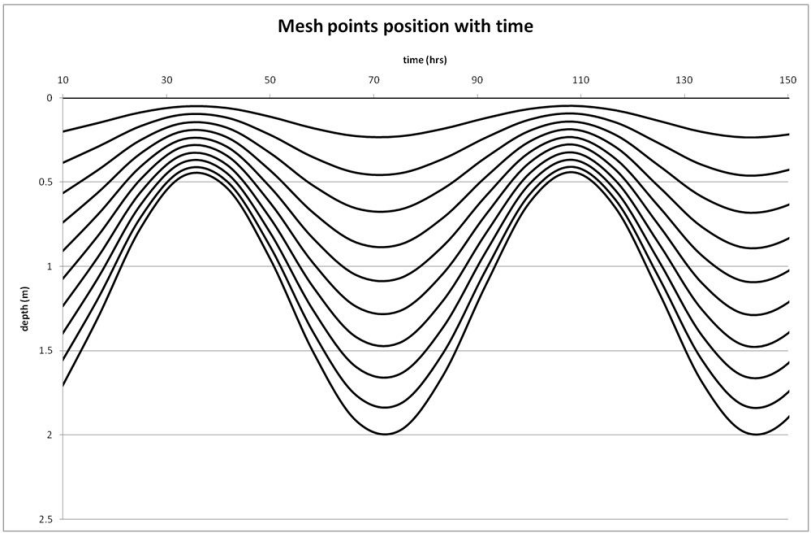

Figure 5.7: Results from moving mesh scheme showing mesh points moving with time.

was calculated for the fixed mesh scheme using the following equation:

$$\text{water balance} = (\text{change in profile water} + \frac{da}{dt}\theta_I + q_0 + q_I)\Delta t = 0 \quad (5.2)$$

where q_I and q_0 are the fluxes at the boundaries, and da/dt is the velocity of the water table. It was found that the LHS of equation (5.2) was of the same magnitude as the individual terms on the RHS. The fixed scheme in this case did not seem to conserve θ whereas this is inherent in the derivation of the moving mesh scheme. For the fixed mesh schemes, the treatment of the

lower boundary could be improved. Currently the last mesh point (I) moves with the water table depth a, so that the spacing between mesh points I and $I+1$ can have values between 0 and Δz where Δz is the original mesh spacing (and equal to the spacings between the other mesh points).

5.2 Infiltration into dry soil

Rain falling onto dry soil will produce large gradients of water below the soil surface. Depending on the intensity of the rain and the type of soil, either unsaturated or saturated (ponded) flow into the soil will result. A fine-textured soil (clays) will have more chance of ponded infiltration since this soil typically has a much lower saturated hydraulic conductivity than coarser sandy soils. If the rainfall rate is greater than the maximum infiltration rate for a particular soil, then saturated or ponded infiltration will occur. From a modelling perspective, the top boundary condition will be a flux or Neumann condition for unsaturated infiltration and a Dirichlet condition for ponded flow.

Unsaturated infiltration

The top boundary condition simulated a constant rain event at a rate of 20 $mm\ day^{-1}$. The initial soil conditions were dry with soil potential equal to $-100m$. Results for the CNi method are shown below in Figures 5.8 and 5.9. Values for Δt for the sandy and clayey soils were both at $3600s$. These values are commonly used in the literature as a compromise between accuracy and efficience [11]. It is also useful to relate Δt to some simple fraction of an hour. From Table 5.1, it is expected that a larger Δt can be used for lower saturated hydraulic conductivity values. The results from the CNi scheme is given by Figures 5.8 and 5.9 for sandy and clayey soils

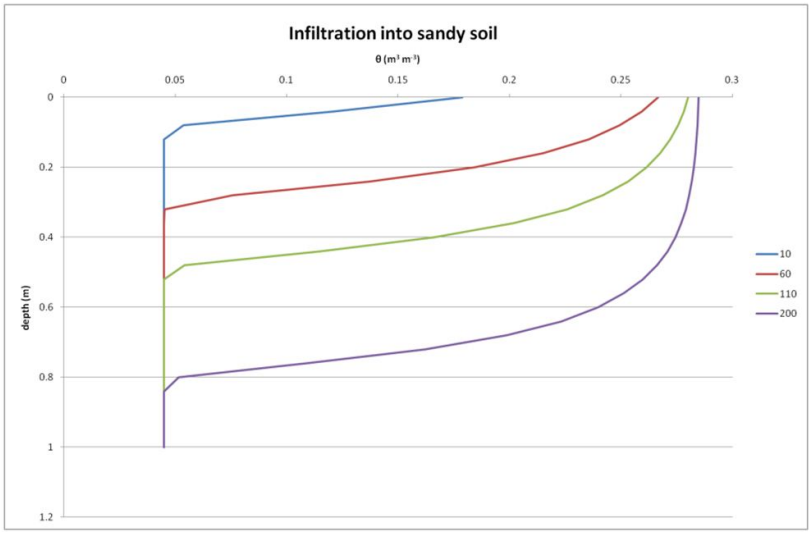

Figure 5.8: Fixed mesh solutions for infiltration onto sandy soil.

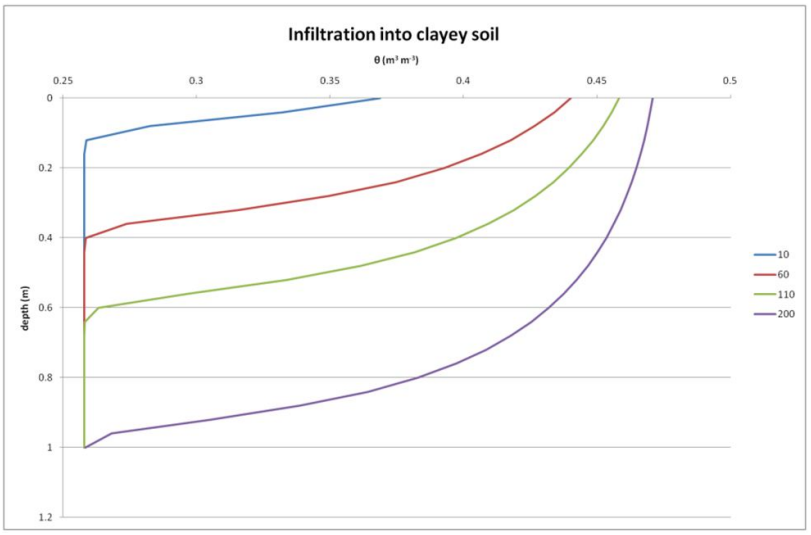

Figure 5.9: Fixed mesh solutions for infiltration onto clayey soil.

respectively with Δt given as $3600s$ for each. Figures 5.8 and 5.9 agree well, with the moving mesh producing slightly faster rate of water infiltration. The number of iterations per timestep as well as the mass balance error is shown in Figures 5.10 and 5.11. In both figures, the initial values for these is high coinciding with initially high moisture gradients. The initially high values quickly decay to low levels as time progresses so an hourly timestep could be suitable here, especially for the finer textured soils. Higher rainfall rates could pose more of a problem which is shown in the next section for ponded infiltration. The results for the MM scheme is given in Figures

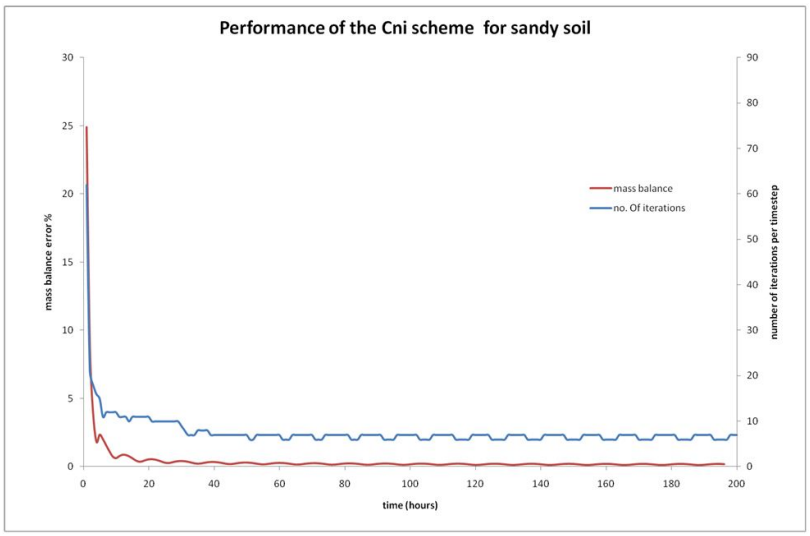

Figure 5.10: Iterations per timestep and % error for the fixed mesh scheme (CNi) for sandy soil.

5.12 and 5.13. These show good similarity with the CNi scheme results with after 100 hours the difference in profile water is 1.4%. The timestep used was $30s$ which is considerably smaller than the CNi scheme since the MM is an explicit scheme. Although not shown here, the time taken per timestep for the MM scheme is likely to be alot less than for the CNi scheme. For

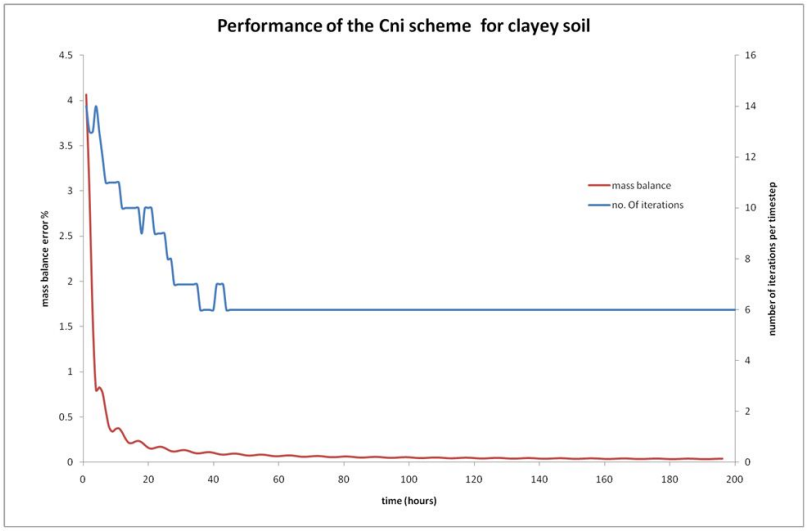

Figure 5.11: Iterations per timestep and % error for the fixed mesh scheme (CNi) for clayey soil.

the latter, the computations include finding the inverse of a $I \times I$ matrix P times, where P is the number of iterations per timestep. Hence the total amount of time for each of the simulations using MM and CNi will be closer than the difference in timesteps suggest.

Ponded infiltration

Initially dry soil ($\psi = -100\ m$) is subjected to ponding with constant depth of 5 mm. The head pressure at the soil surface (ψ_0) is therefore equal to 0.005 m. This situation creates very large initial gradients near the soil surface as water begins to infiltrate. This will have a big influence on the size of Δt for the schemes to produce stable and accurate solutions. Figures 5.15 and 5.16 shows the output of the CNi scheme for the sandy and clayey soils respectively. Figures 5.17 and 5.18 giving the iterations per timestep. The Δt used for the CNi scheme is 0.25 s and 1 s for sandy and clayey

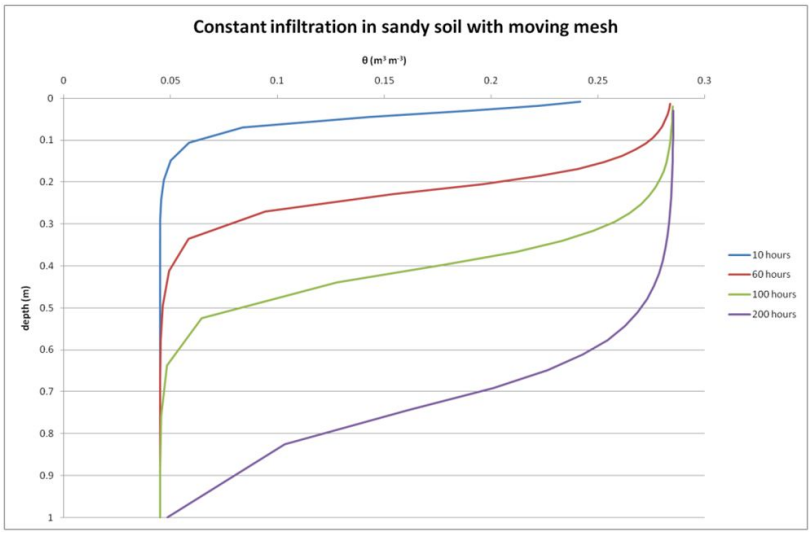

Figure 5.12: Moving mesh solutions for infiltration onto sandy soil.

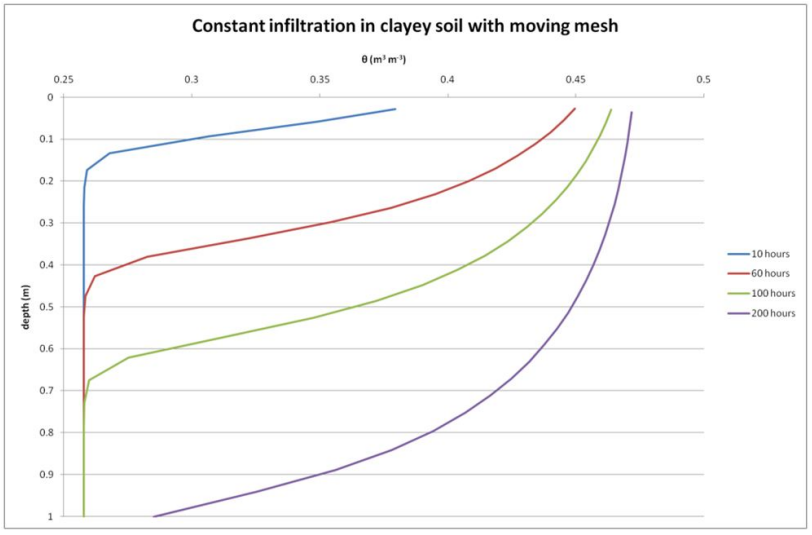

Figure 5.13: Moving mesh solutions for infiltration onto clayey soil.

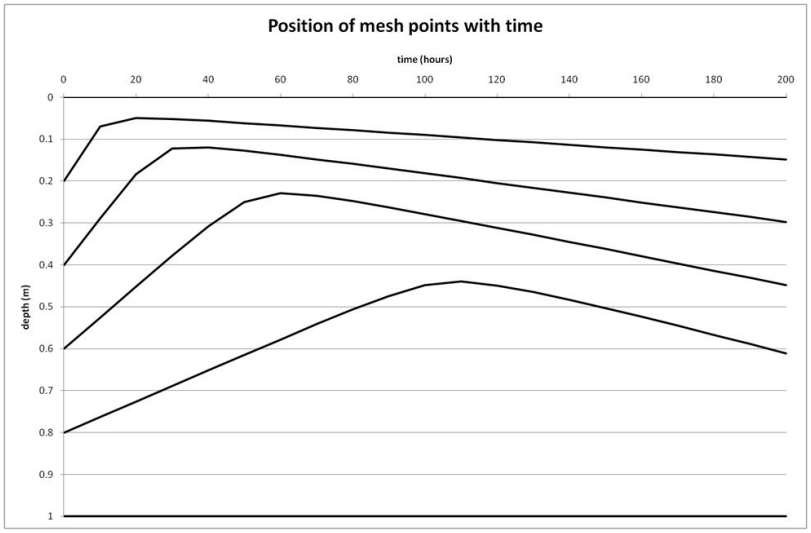

Figure 5.14: Results from moving mesh scheme showing mesh points moving with time (sandy soil).

soils respectively because the scheme would not run at timesteps much larger than these. The very small values of Δt used reflects on the size of the initial gradients resulting from a positive head pressure boundary condition. For ponded infiltration in particular, a small Δt is required initially and then can be increased as the water infiltrates and gradients lessen. This situation would be ideally suited to have an adaptive timestep method included in the scheme. The results for the moving mesh scheme is shown in Figures 5.19 and 5.20. The ponded infiltration into both soils shows reasonably good agreement between the schemes with the amount of water infiltrated (or depth to the wetting front) slightly less for the moving mesh. Table 5.3 summarises the % difference between the schemes. The moisture gradient at the wetting front with the MM scheme is considerably sharper than that from the CNi method. Sharp wetting fronts are well documented under ponded conditions ([12] and [13]). The MM scheme is

Table 5.3: % error values in profile water between schemes.

time(hr)	% error sand	% error clay
1	27.5	6.9
2	19, 4	7.2
3	14.9	6.9
4	11.0	6.1
5	8.1	5.3

better here at capturing the piston-like effect of ponded infiltration.

One of the reasons for differences between the schemes is the SMC relation used. It was preferred here to use the Brookes-Corey relation as shown in Chapter 2. The procedure for simulating the infiltration of water in the fixed mesh scheme was to set $\psi(0) = 0.005$ and the scheme run with Darcy's Law determining the water infiltrated through the soil surface:

$$q_0 = -K_{1/2}\frac{\psi_1 - h - L}{L} \tag{5.3}$$

where $L = \Delta z_1$ initially, and Δz_1 is the spacing between z_0 and z_1. Each time a mesh point i immediately below the wetting front became greater than ψ_e, we set $\psi_i = \psi_e$ and $L = L + \Delta z_i$, and the scheme was advanced. So the value of ψ_e will have some influence on the speed of the infiltrating front. This is probably a weakness in using this particular SMC relation and a better relation which deals with the SMC near saturation [3].

5.3 Infiltration into layered soil

Almost all soil profiles consist of layers of different soil types, which often can be very distinctive layers with large differences in soil properties. To simulate vertical water movement in layered soil, ψ-based RE must be used since the value of ψ remains continuous down the profile. In contrast, θ will

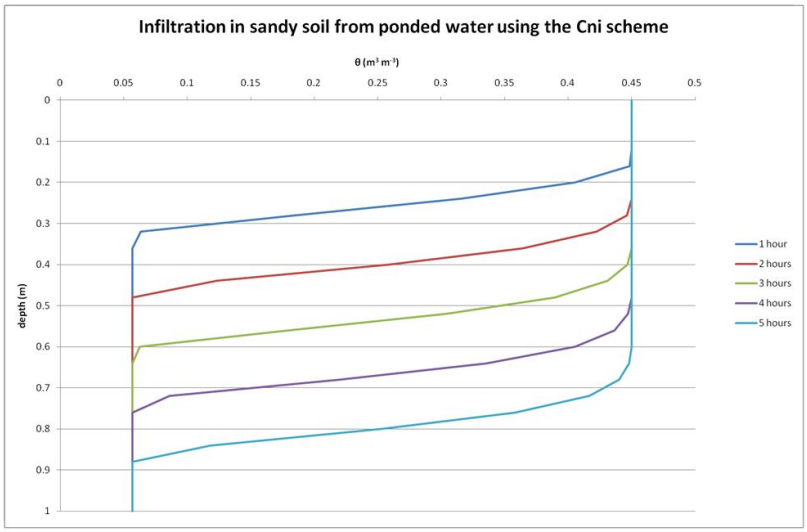

Figure 5.15: Fixed mesh solutions for ponded infiltration onto sandy soil.

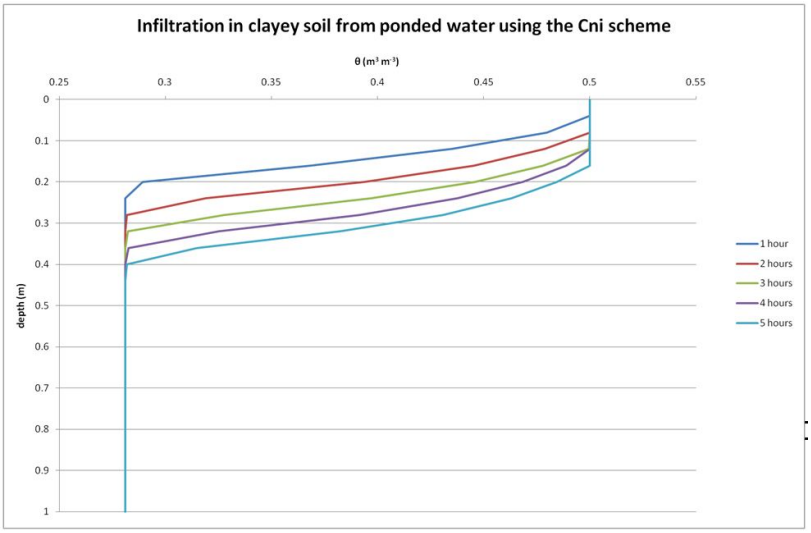

Figure 5.16: Fixed mesh solutions for ponded infiltration onto clayey soil.

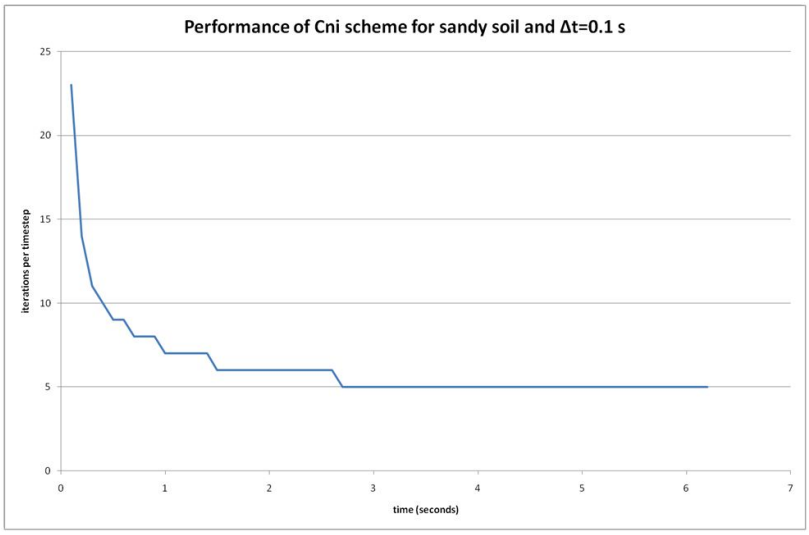

Figure 5.17: Iterations per timestep for the CNi scheme for the sandy soil

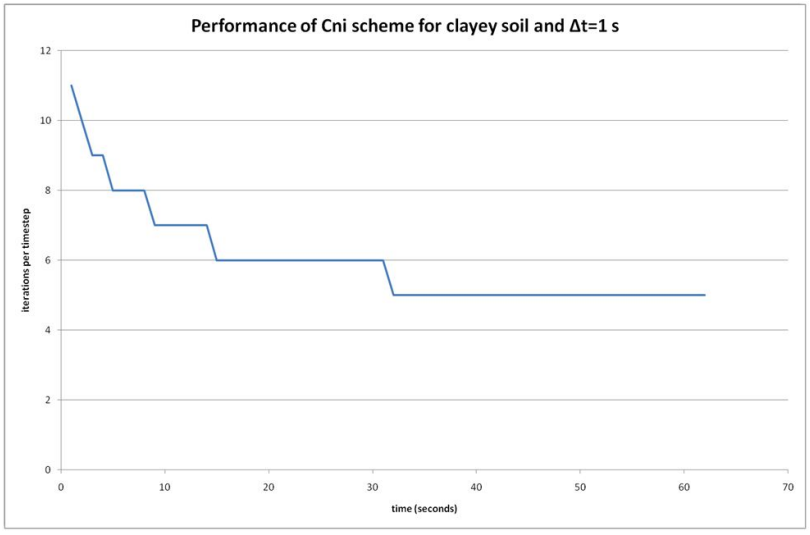

Figure 5.18: Iterations per timestep for the CNi scheme for the clayey soil

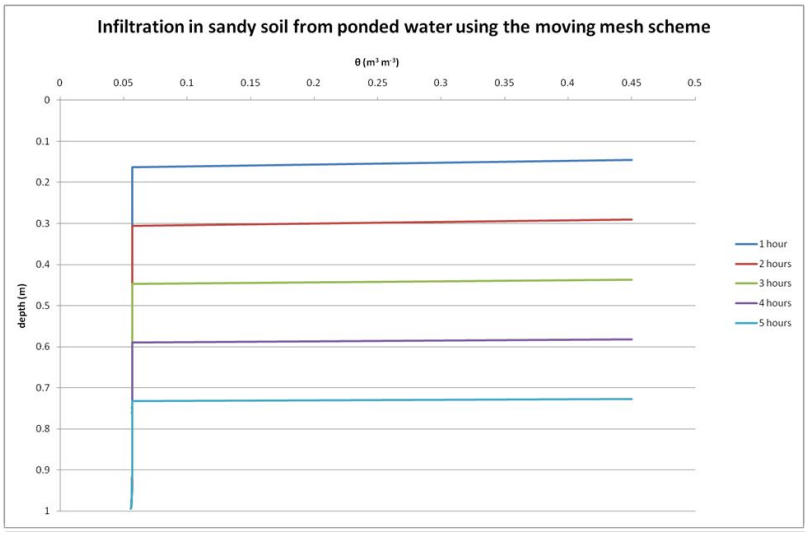

Figure 5.19: Moving mesh solution for ponded infiltration onto sandy soil.

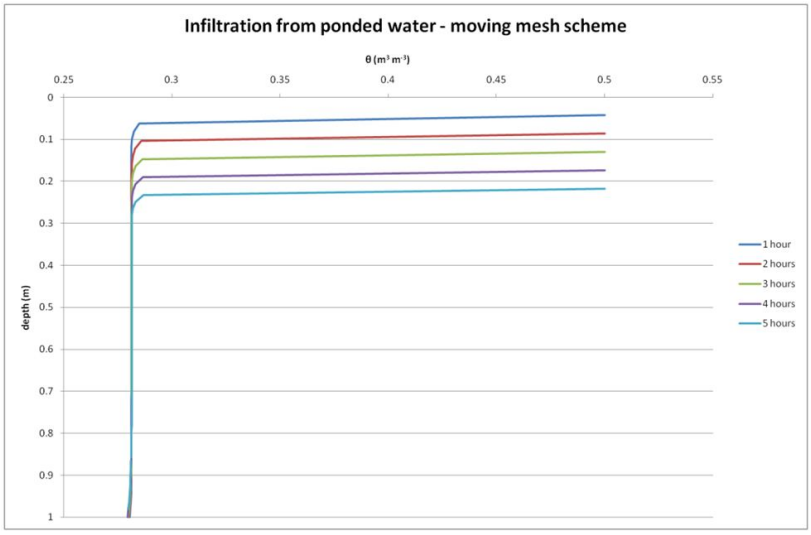

Figure 5.20: Moving mesh solution for ponded infiltration onto clayey soil.

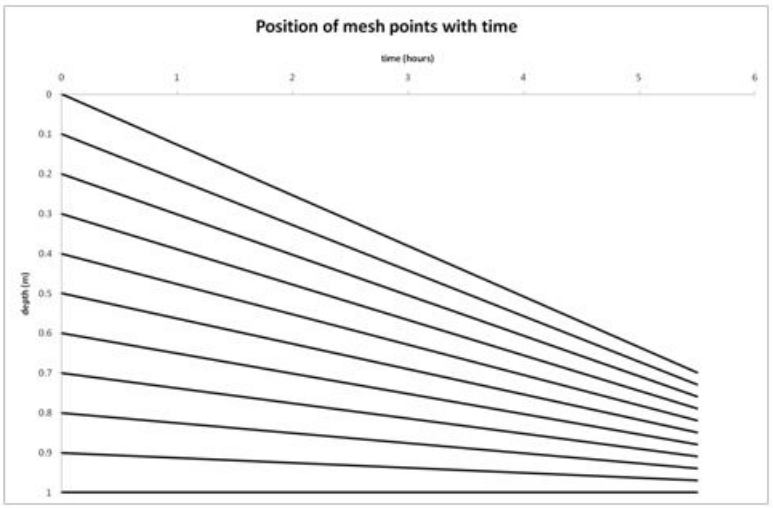

Figure 5.21: Moving mesh solution for sandy soil showing position of mesh points with time.

generally have large discontinuities in value down a layered profile. Here a soil with two contrasting soil layers; clay over sand, initially dry, is subjected to continuous infiltration at 20 $mm\ hr^{-1}$. The clay over sand soil profile was chosen as this situation can cause the wetting front (under moderate infiltration rates) to be held up [14]. This causes the moisture gradient at the clay/sand boundary to become steeper. Unstable flows can result which culminate in 'fingered flows' through the sand. This greatly enhances the rate of flow of water further down the profile which has implications for leaching of contaminants into the groundwater [15].

The MM scheme for the whole profile would not be useful with a stationary boundary in the middle of the profile. So two types of methods were investigated here, (i) a fixed mesh is inserted on the whole soil profile, and (ii) a moving mesh was placed on the top soil and a fixed mesh on the bottom soil layer. Figure 5.22 shows the results from the fixed mesh method.

The mass balance error is calculated by comparing the input of water to the simulated change in profile water content (Table 5.4) which shows after an initial value of 8.9% decreases quickly. This value remained under 1% for the remainder of the simulation even when the wetting front passed through the soil profile discontinuity. Figure 5.23 shows results from the second

Table 5.4: % Mass balance error for CNi scheme.

time(hr)	% error
1	8.9
2	3.0
3	1.1
4	1.1
5	0.9

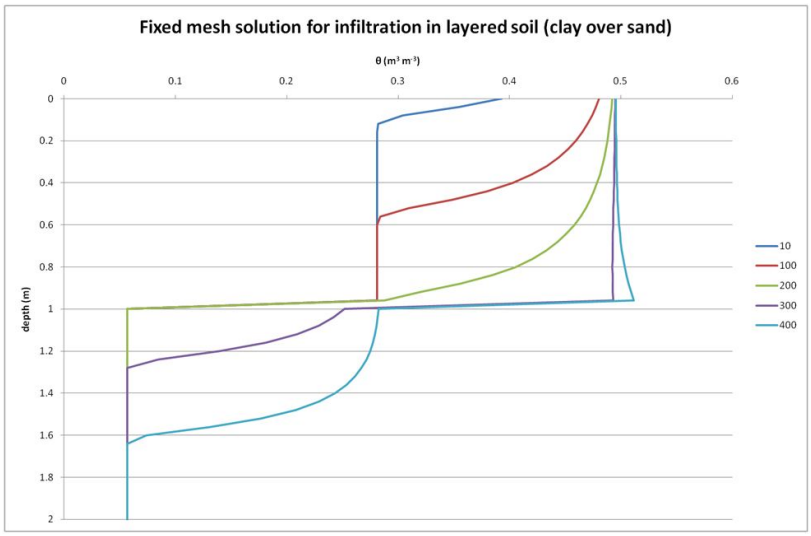

Figure 5.22: Fixed mesh solution for infiltration into layered soil; clayey over sandy soil. Time in hours listed on right

method which is similar to the CNi only method. A considerably smaller timestep was required for the second method (30 s compared to 3600 s)

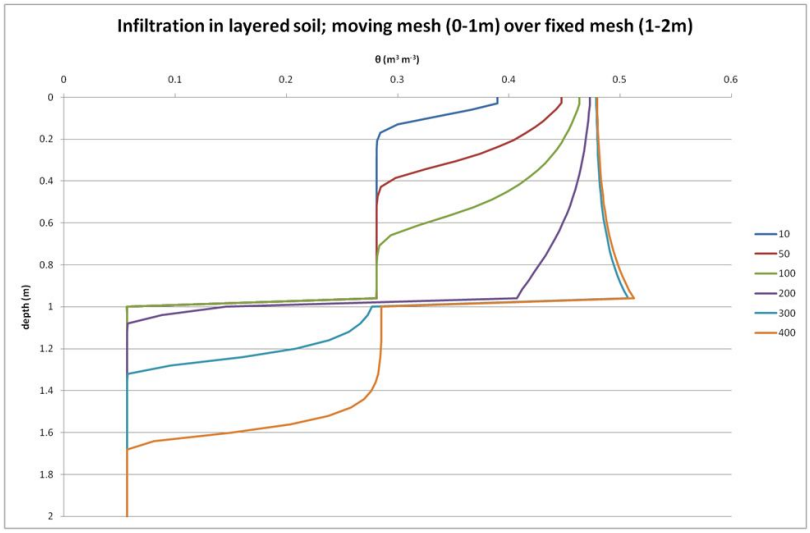

Figure 5.23: Moving mesh solutions for infiltration into layered soil; clayey over sandy soil. Time in hours listed on right

since the MM scheme is explicit. The potential for the MM scheme to be used at the boundary to improve the treatment of the gradients is investigated further in the next chapter. As water builds up at the boundary and the moisute gradient increases, the spacing between the mesh points contract so enhancing the resolution. The potential for the MM scheme to be used at the boundary to improve the treatment of the gradients is investigated further in the next chapter.

6 Investigation into waiting times

Vertical flow only is considered in the following analysis. It has been found in practice that water infiltrating into soil at a 'medium' rate (a rate sufficiently below the maximum rate so gravity forces are not dominating, and high enough so matric forces are not dominating) can cause unstable flows at the wetting front. This is common in layered soils where a fine-textured soil overlies a coarse-textured one. In this case, the advance of water is held up at the boundary of these two soil types and after some time breaks through the boundary in 'fingers' of flow. This has also been observed within coarse-textured soils which are initially dry and then subjected to water infiltration. In both cases there is a period of time where the wetting front is stationary followed by water flow through this point, resulting in 'fingered' flow. Water flow in soil is governed by Darcy's Law:

$$q = -K\left(\frac{\partial\psi}{\partial z} + 1\right) \tag{6.1}$$

where the hydraulic conductivity (K) is given here as:

$$K = K_s\left(\frac{\theta}{\theta_s}\right)^n \tag{6.2}$$

The relationship between water potential (ψ) and water content (θ) is given here as:

$$\left(\frac{\psi}{\psi_e}\right) = \left(\frac{\theta}{\theta_s}\right)^{-b} \tag{6.3}$$

where ψ_e, θ_s, b, and n are constants and $n = 2 + 3b$. If we now consider equation (6.1) with θ only as the independant variable, using the chain rule and differentiating equation (6.3) with respect to θ, equation (6.1) becomes:

$$q = -(A\theta^{n-b-1}\theta_z + B\theta^n) \tag{6.4}$$

where $A = -bK_s\psi_e\theta_s^{b-n}$ and $B = K_s\theta^{-n}$. Hence the Darcy velocity (v) is given by:

$$v = -(A(\theta^{n-b-1})_z + B\theta^{n-1}) \tag{6.5}$$

For the purposes of investigating this 'waiting' behaviour of the wetting front discussed above, the constants in equation (6.5) are set to unity with $b = 2$ giving:

$$v = -(\theta^5)_z - \theta^7 \tag{6.6}$$

and the initial conditions are given by

$$\theta = \begin{cases} (1-z)^\alpha & \text{if } z \leq 1, \\ 0 & \text{if } z > 1 \end{cases}$$

with $\alpha = 1$, consistent with the boundary condition. The Darcy velocity $v > 0$ for $z < 1$ and $v = 0$ at $z = 1$. From equation (6.6) ,for v to become greater than zero at $z = 1$, θ_z must become infinite at that point. Figure 6.1 shows the initial conditions with the equivalent of normalised θ and then at some time T where the gradient has increased by decreasing α. The behaviour of the v when $\theta_z \to \infty$ is now investigated further by substituting the initial conditions into equation (6.6) giving:

$$v = 5\alpha(1-z)^{5\alpha-1} - (1-z)^{7\alpha}. \tag{6.7}$$

As time advances, the value of α will decrease and at $z = 1$, there are three possible outcomes for v depending on the value of α:

1. for $5\alpha < 1$, $\quad v \to \infty$

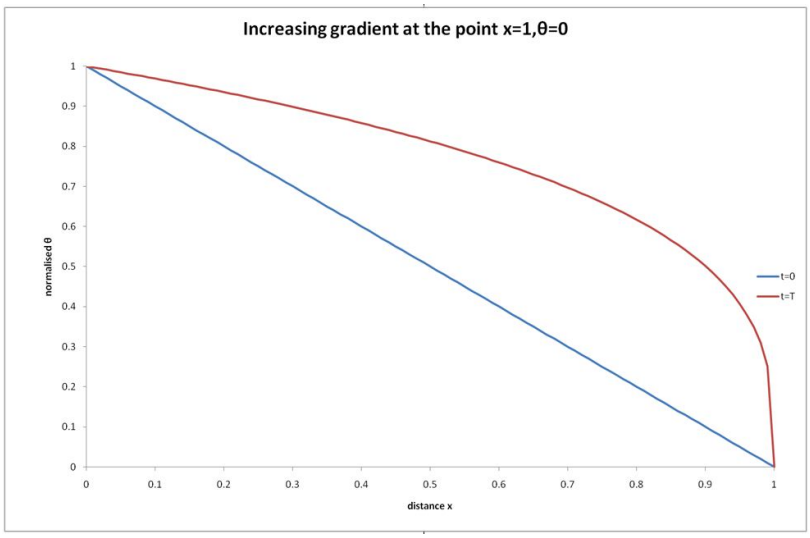

Figure 6.1: Gradient at the point $x = 1$ at t=0 and increasing at time t=T in response to α decreasing from 1 to 0.3.

2. for $5\alpha > 1$, $v \to 0$

3. for $5\alpha = 1$, v is finite

Hence, when the shape of the wetting front changes, α decreases until case (3) above is reached when v at $z = 1$ becomes finite and moves in the direction of increasing z.

When solving the problem above numerically using a velocity-based moving mesh technique, the mesh points are required to move according to the discrete form of equation (6.8):

$$\left.\frac{\partial z}{\partial t}\right|_i \approx \frac{z_i^{n+1} - z_i^n}{\Delta t} = \frac{\theta^5_{i+\frac{1}{2}} - \theta^5_{i-\frac{1}{2}}}{z_{i+\frac{1}{2}} - z_{i-\frac{1}{2}}} - \theta_i^7 \tag{6.8}$$

The value of θ at mesh point $z = 1$ $(i = I)$ is not zero but a small value termed the residual or minimum value, here its $0.01m^3m^{-3}$. The mesh point I will therefore initially have a very small velocity. Eventually the velocity will become noticeably greater once the moisture gradient at point

I increases and this is shown in Figure 6.2. The mesh points near point I decrease with time as shown in Figure 6.3 and this is useful in simulating the large (infinite in theory) gradient necessary at point I for velocity to increase appreciably above zero. The numerical solution does therefore appear to mimic the analytical analysis above.

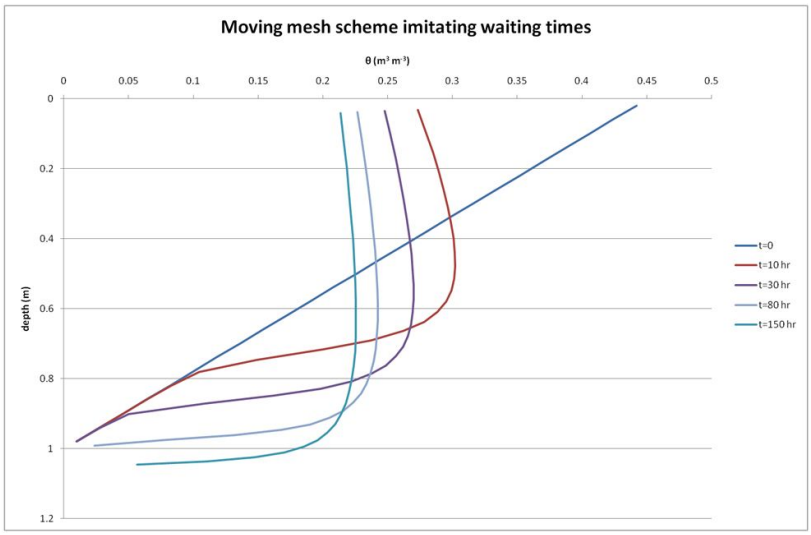

Figure 6.2: Moving mesh scheme mimicing the waiting time as predicted from theory.

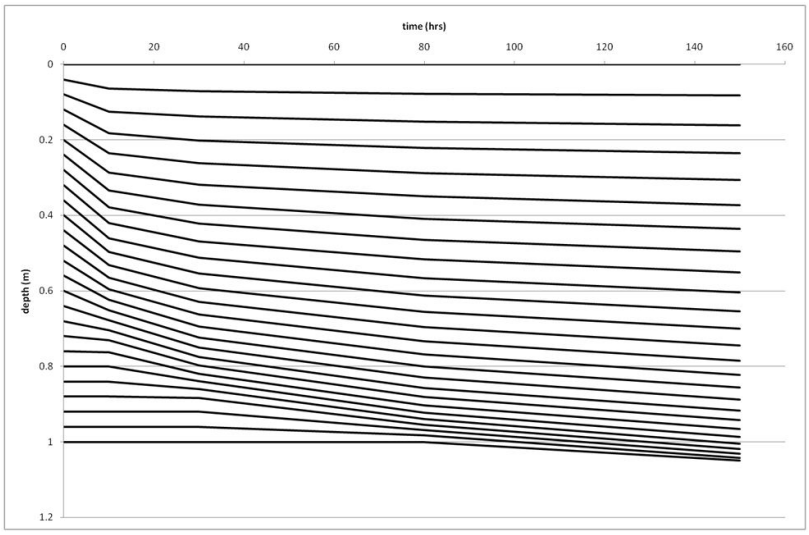

Figure 6.3: Mesh points position with time. The spacings decrease dramatically near point I as the velocity at I noticeably increases.

7 Conclusions and Future work

7.1 Conclusions

In this report two different schemes were formulated to numerically solve the Richards' equation for vertical soil water flow; a fixed mesh scheme and a moving mesh scheme. The fixed mesh scheme used here was the nonlinear Crank-Nicolson scheme (with a Newton iteration), CNi, where the diffusion parameters were evaluated at the $n + 1$ level. The moving mesh scheme MM, was based on a conservation principle where the fractional amount of moisture between adjacent mesh points remained constant for all time. This allowed the mechanism for moving the mesh points to be determined.

The two schemes were applied to four scenarios:

(i) shallow moving water table

(ii) unsaturated infiltration onto dry soil

(iii) ponded infiltration onto dry soil

(iv) unsaturated infiltration onto layered soil

The CNi scheme has been a proven performer for many years with solving for soil water flows but recently more sophisticated schemes have been developed. The question here is: is the CNi scheme robust enough to deal with the scenarios above? The accuracy required and computational

resource available will determine the answer. Except for the ponding infiltration problem, the CNi scheme performed well with an hourly timestep with some minimal loss in accuracy. Shorter timesteps could be used for the initial gradients from infiltration and longer thereafter. The ponded case required the timestep to be dramatically reduced in order for the scheme to run at all. So for this extreme case, an adaptive timestep procedure is necessary, so once the initial stages of the ponding infiltration has taken place (first few minutes), the timestep can be increased so as not to overly tax the computation resources especially when simulating large time periods (e.g. several years in duration).

The MM scheme proved useful in the first three scenarios, especially where there are free or moving boundaries. It compared well with the CNi scheme, but although requiring a much smaller timestep, the simplicity of the MM scheme will mean less compuation time per timestep. The MM scheme is inherently conservative, so overall could have some benefit in cetain situations to solving for soil water flows.

Finally the onset of unstable flows were investigated and a possible mathemtical mechanism developed to explain the observed waiting times found in other studies. The MM scheme was implemented and found to mimic the waiting time predicted in theory by simulating the very steep gradient close to the zero velocity point.

7.2 Future work

Several interesting avenues of work could be followed on the back of this report:

(i) Improve the robustness of the CNi model implemented in this report by incorporating a adaptive timestepping scheme. This could be achieved

by either an empirical approach based on the number of iterations per timestep or using a mechanistic approach which is based on an estimate of the truncation error at each timestep [17]. This adaptive scheme could be simply added with little internal change to CNi scheme.

(ii) An existing study on the Oxfordshire floodplains (joint project by the University of Reading and CEH Wallingford) has as one of its objectives to develop a combined soil water and heat flow model which is to interface with an existing above-ground water and energy balance model. The work done here to implement a robust implicit finite difference scheme for solving Richards' equation could be further advanced to incorporate a coupled heat and vapour flow model. The full system of equations is [16]:

$$C\frac{\partial\psi}{\partial t} = \frac{\partial}{\partial z}\left[(K+D_v)\frac{\partial\psi}{\partial z}+D_T\frac{\partial T}{\partial z}+K\right]-S \qquad (7.1)$$

$$C_H\frac{\partial T}{\partial z} = \frac{\partial}{\partial z}\left[\lambda\frac{\partial T}{\partial z}+\rho_w L D_v\frac{\partial\psi}{\partial z}\right]-c_w\theta\frac{\partial T}{\partial z} \qquad (7.2)$$

where D_v is the isothermal vapour conductivity (ms^{-1}), D_T is the thermal vapour diffusivity ($m^2s^{-1}K^{-1}$), S is the extraction of water from the roots, C_H is the volumetric heat capacity of the soil ($Wm^{-3}K-1$), λ is the thermal conductivity of the soil ($Wm^{-1}K^{-1}$), ρ_w is the density of water (kgm^{-3}), L is the latent heat of vapourisation (Jkg^{-1}), and c_w is the thermal conductivity of water ($Wm^{-1}K^{-1}$). One way to implement equation 7.2 is to follow the procedure of [11] and have separate procedures for each of water, vapour, and heat flows inside an iterative procedure.

(iii) Other interesting possibility would be implement an implicit version

of the moving mesh scheme to allow larger timesteps to be taken.

(iv) It would be a very useful exercise to improve the programs so as to make them more modular in design. This then will make them more transferable in their application to other problems such as that in (ii) above.

Bibliography

[1] Dr. Anne Verhoef, School of Human and Environmental Sciences, University of Reading

[2] Brookes R.H. and Corey A.T. Hydraulic properties of porous media: Hydrology Papers, Colorado State University, 24 pages,1964

[3] van Genutchen M.Th. A closed-form equation for predicting the hydraulic conductivity of unsaturated soils. *Soil Sci. Am. J.* 44:892-898, 1980

[4] T.P. Clement, W.R. Wise, F.J. Molz. A physically-based, two dimension finite difference algorithm for modelling variably saturated flow. *J. of Hydrol* 161, 71-90, 1994

[5] Miller C.T., Abhishek C., M.W. Farthing. A spatially and temporally adaptive solution of Richards' equation. *Adv. in Water Res.* 29: 525-545, 2006

[6] Williams G.A. and C.T. Miller. An evaluation of temporally adaptive transformation approaches for solving Richards' equation. *Adv. in Water REs.* 22(8) 831-840, 1999

[7] Dale Partridge. Analysis and computation of a simple glacier model using moving grids. *University of Reading MSc dissertation*, 2009

[8] Kam Wong. Accuracy of a moving mesh numerical method applied to the self-similar solution of nonlinear PDEs. *University of Reading MSc dissertation*, 2010

[9] Raff D.A. and J.A. Ramirez. A physical, mechanistic and fully coupled hillslope hydrlogy model. *Int. J. Meth. Fluids* 49: 1193-1212,2005

[10] Kylie Osman. Numerical schemes for a nonlinear diffusion problem. *University of Reading MSc dissertation*, 2005

[11] Daamen C. and L. Simmonds. Soil Water, Energy and Transpiration, A numerical model of water and energy fluxes in the soil profile and sparse canopies. *Department of Soil Science, University of Reading*, 1994

[12] Hillel D. Introduction to soil physics. *Academic Press Inc.* 392 pages, 1982

[13] Asawa G.L. Irrigation and Water Resouces Engineering. *New Age Int.* 624p, 2006

[14] de Rooij G.H. Modelling fingered flow of water in soils owing to wetting front instability: a review. *J. of Hydrol.* 231-232:277-294, 2000

[15] Nieber J.L. Numerical simulation of experimental gravity-driven unstable flow in water repellent sand. *J. of Hydrol.* 231-232: 295-307, 2000

[16] Milly, P.C.D. Moisture and heat transport in hysteretic inhomogeneous porous media: a matric headbased formulation and a numerical model. *Water Resour. Res.*, 18:489-498, 1982

[17] Kavetski D., P. Binning. and S. W. Sloan. Adaptive backward Euler time stepping with truncation error control for numerical modelling of unsaturated fluid flow. *Int. J. Numer. Meth. Engng* 2002; 53:13011322